Inductive Interferences Between a 500 kV Power Line and a Pipeline with a Complex Approximation Layout and Multilayered Soil

Amauri G. Martins-Britto, Caio M. Moraes, Felipe V. Lopes

***Abstract*—This paper presents a steady-state electromagnetic interference study between a 500 kV overhead transmission line and a neighboring pipeline, based on data from a real project with a complex geometry and with emphasis on how the soil structure affects the inductive coupling mechanism, as well as the effectivity of grounding devices to reduce potentially hazardous pipeline induced voltages. Soil parameters are determined from actual field measurements, which results in a soil model composed of three layers. Conductor impedances are computed using a modification of the original Carson equation, in which the term describing the soil resistivity is replaced by an equivalent uniform of the multilayered structure, and then a circuit model is built using the Alternative Transients Program (ATP) to predict the resulting induced voltages. Results show an excellent agreement between the proposed approach and the reference values, with a comprehensible evaluation of the risks to which the interfered pipeline is exposed and how to mitigate them.**

***Keywords*—Electromagnetic interferences, inductive coupling, pipelines, soil resistivity, transmission lines.**

I. Introduction

An underground pipeline made of conductive material, when exposed to the magnetic field surrounding the energized phases of a transmission line, is subjected to a variety of effects, which cause the rise of the metal potential along its course, due to the inductive coupling mechanism between the two installations.

Induced voltages depend on the geometry of structures, type and arrangement of conductors, current magnitude, type of pipeline coating and soil electrical resistivity, among other factors. Such voltages pose potential risks to the integrity of facilities and people involved, for instance: electrical shock caused by touch voltages, breakdown of the pipeline dielectric coating, electrochemical corrosion of the metal and damage resulting of current imposition to the metallic pipe and connected equipment [1].

The first formal studies of EMI involving power lines and pipelines date back to 1978, in the United States, with the technical report EL-904 [2], [3] and the subsequent works by Dawalibi *et al.* [4], who developed a generalized approach to analyze the effects of transmission line faults on natural gas pipelines, based essentially on the contributions provided by Carson [5], Pollaczek [6], Sunde [7] and Heppe [8], which form the basis of what has become the industry standard up to date.

With the increasing computational power, multilayered soil models have become a topic of attention among researchers interested in inductive coupling phenomena [9], [10], [11]. Currently, the state-of-the-art in EMI research involves the study of the transient behavior of complex geometries and convoluted soil heterogeneities, with successful reports of applications using the FDTD method [12], [13], as well as finite element analysis [14], [10].

The idea of using EMTP-type tools to carry out EMI simulations has been explored successfully by several researchers, and even the well-known ATP is reported to feature specific routines to predict interference levels caused by inductive coupling on a target line [15]. However, EMTP-based studies available in the literature are mostly limited to small systems, parallel approximations and uniform soil structures [16], [17], [18].

In this context, the soil structure plays a fundamental role and is a recognized source of uncertainties [19]. Natural soils are highly variable in their properties and seldom homogeneous. However, its influence in the classic coupling model is represented, in Carson equation, by a semi-infinite medium with uniform resistivity, despite the fact that most soils are reported to be multilayered structures [5], [20]. Moreover, real life transmission systems and pipelines are complex installations that may span for several kilometers and follow arbitrary paths, which are determined by engineering constraints such as topography/terrain characteristics, environmental regulations, land expropriation etc.

Because of this gap in the literature, there is potential for enhancement of the current EMTP-based modeling techniques, so that N-layered soil models are represented accurately, as well as generalization for arbitrary approximation geometries between the source and target systems, which are the main contributions this work is expected to offer.

The authors present a real interference case between a 500 kV transmission line and a 28" gas pipeline, with a complex approximation layout, composed of oblique sections and one crossing point, and soil parameters determined from actual resistivity surveys. Induced voltages are calculated using an improved equivalent circuit approach implemented in the EMTP/ATP, leveraging a technique recently proposed by the authors, in which the multilayered property of real soils is

The authors gratefully acknowledge the financial support of PNPD/CAPES.
A. G. Martins-Britto, C. M. Moraes and F. V. Lopes are with University of Brasília, Distrito Federal, Brazil (e-mail: amaurigm@lapse.unb.br; caio.missiaggia@aluno.unb.br; felipevlopes@unb.br)
Paper submitted to the International Conference on Power Systems Transients (IPST2021) in Belo Horizonte, Brazil June 6-10, 2021.

accurately modeled using the traditional Carson equation [21], [22].

Of practical interest to industrial applications and broadening research possibilities to various relevant topics, this work demonstrates how to build complex, realistic interference models, using conventional techniques and tools, aiming at the prediction and mitigation of risks to which people and pipelines are exposed, thus assisting in the design of safer facilities.

II. Mathematical Model

A. Inductive coupling mechanisms

Fig. 1 describes a system composed of two parallel conductors above a semi-infinite uniform, which represents the fundamental block for building interference models composed of crossings and/or oblique approximations, as complex geometries can be split into several cells expressed in terms of equivalent parallelisms [1].

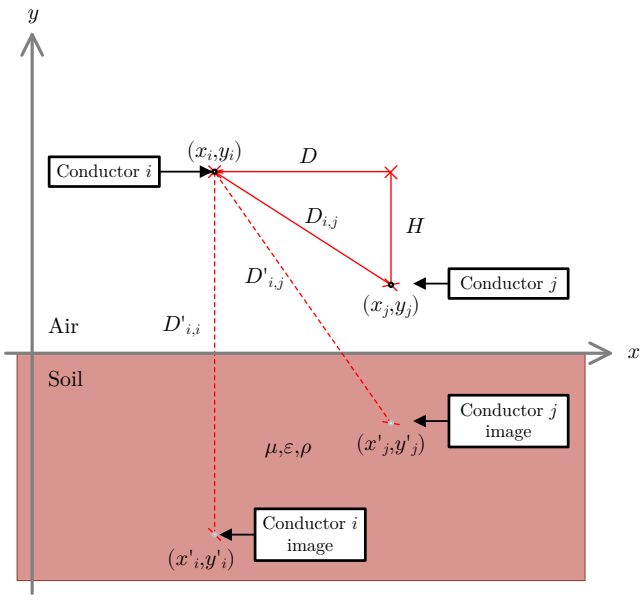

Fig. 1: Two overhead conductors above a semi-infinite uniform ground and its images.

If the energized conductor carries a current I, the resulting magnetic field in the vicinities of the exposed conductor induces electromotive forces given by (1):

$$E = Z_m \times I, \tag{1}$$

in which E is the induced electromotive force, given in volts; I is the source current, in ampères; and Z_m is the mutual impedance between conductors i and j with ground return path, computed in ohms per unit length using Carson equation (2) [5]:

$$Z_{i,j} = Z_m = \frac{j\omega\mu_0}{2\pi} \ln\left(\frac{D'_{i,j}}{D_{i,j}}\right) + \frac{j\omega\mu_0}{2\pi} \int_0^\infty \frac{2e^{-H\lambda}}{\lambda + \sqrt{\lambda^2 + j\frac{\omega\mu_0}{\rho} - \omega^2\mu_0\varepsilon_0\varepsilon_r}} \cos(\lambda D)\, d\lambda, \tag{2}$$

in which $\mu_0 = 4\pi \times 10^{-7}$ H/m is the magnetic permeability constant of free space; $\varepsilon_0 \approx 8.85 \times 10^{-12}$ F/m is the vacuum electrical permittivity; ρ is the local soil electrical resistivity, in Ω.m; ε_r is the local soil relative electrical permittivity; H, D, $D_{i,j}$ and $D'_{i,j}$ are the relative distances represented in Fig. 1, in meters, with: $H = |y_i - y_j|$, $D = |x_i - x_j|$, $D_{i,j} = \sqrt{(x_i - x_j)^2 + (y_i - y_j)^2}$ and $D'_{i,j} = \sqrt{(x_i - x'_j)^2 + (y_i - y'_j)^2}$.

The first term in (2) represents the ground return impedance for a perfectly conductive soil. The improper integral, known as Carson's integral, introduces the effects of the soil with finite resistivity, including losses caused by current return. The solution to Carson's integral has been studied by several authors, using techniques based on numerical integrations, power series expansion or deduction of simplified expressions, being worth mentioning the adaptive series implemented in the Line/Cable Constants ATP routine [12], [23].

It happens, however, that most real soils are layered media, frequently composed of three to five layers [20]. Carson's integral for a soil model composed by N layers has been derived by Nakagawa *et al.*, resulting in a complex recursive solution, with successive products of exponential terms on the integration variable λ, prone to errors and numerical instabilities, due to its oscillating form [9], [10]. Working with arbitrary soil structures requires specific techniques which are not always readily available in software commonly used in power systems analysis. To overcome this difficulty, a workaround is described in the next section.

B. Multilayer soil approximation by an equivalent uniform

In the following discussion, conductivity σ and resistivity $\rho = 1/\sigma$ are employed indistinctively for the sake of legibility of the presented equations.

Assuming a N-layered soil structure, with respective permeabilities μ_n, permittivities ε_n, conductivities σ_n (or resistivities ρ_n) and thicknesses h_n, with $n = 1, 2, ..., N$, as illustrated in Fig. 2, and f being the power system frequency, in hertz, the authors have derived, in a previously published work, an equivalent uniform model, suitable for working with earth return impedances within the frequency range from 60 Hz up to 1 MHz [21].

The presence of multiple layers with different constitutive properties is accounted by replacing the uniform variable σ in Carson equation by the equivalent parameter σ_{eq}, defined as in (3)-(5).

$$\sigma_{N-1,N} = \sigma_{N-1}\left[\frac{(\sqrt{\sigma_{N-1}}+\sqrt{\sigma_N})-(\sqrt{\sigma_{N-1}}-\sqrt{\sigma_N})e^{-2h_{N-1}\sqrt{\pi f\mu_{N-1}\sigma_{N-1}}}}{(\sqrt{\sigma_{N-1}}+\sqrt{\sigma_N})+(\sqrt{\sigma_{N-1}}-\sqrt{\sigma_N})e^{-2h_{N-1}\sqrt{\pi f\mu_{N-1}\sigma_{N-1}}}}\right]^2, \tag{3}$$

$$\vdots$$

$$\sigma_{m-1,m} = \sigma_{m-1}\left[\frac{(\sqrt{\sigma_{m-1}}+\sqrt{\sigma_{m-1,m}})-(\sqrt{\sigma_{m-1}}-\sqrt{\sigma_{m-1,m}})e^{-2h_{m-1}\sqrt{\pi f\mu_{m-1}\sigma_{m-1}}}}{(\sqrt{\sigma_{m-1}}+\sqrt{\sigma_{m-1,m}})+(\sqrt{\sigma_{m-1}}-\sqrt{\sigma_{m-1,m}})e^{-2h_{m-1}\sqrt{\pi f\mu_{m-1}\sigma_{m-1}}}}\right]^2, \tag{4}$$

$$\sigma_{eq} = \sigma_1\left[\frac{(\sqrt{\sigma_1}+\sqrt{\sigma_{m-1,m}})-(\sqrt{\sigma_1}-\sqrt{\sigma_{m-1,m}})e^{-2h_1\sqrt{\pi f\mu_1\sigma_1}}}{(\sqrt{\sigma_1}+\sqrt{\sigma_{m-1,m}})+(\sqrt{\sigma_1}-\sqrt{\sigma_{m-1,m}})e^{-2h_1\sqrt{\pi f\mu_1\sigma_1}}}\right]^2, (1 \le m \le N-2). \tag{5}$$

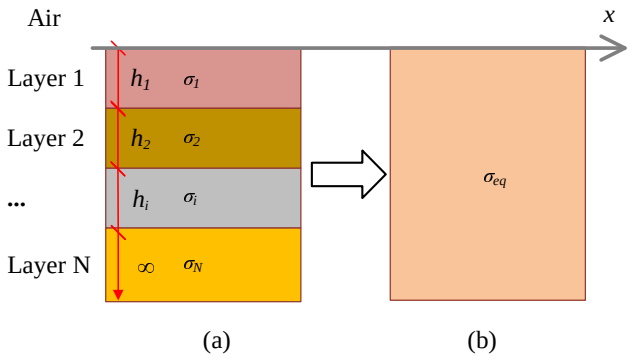

Fig. 2: N-layered soil model and its equivalent uniform.

This approach has been proved to provide accurate results, with the advantage that a much simpler expression is employed, in comparison with the general analytical solution by Nakagawa *et al.*, yielding a single real-valued parameter that can be readily used with the classic Carson equation (2), therefore being fully compatible with the native ATP routines that handle transmission line parameters [9], [21].

C. Parameters of a buried insulated tubular conductor

The EMF induced on the target pipeline, calculated according to (1)-(2), causes current flow along the interfered conductor. For a coated tubular conductor (a pipe), shown in Fig. 3, part of this current leaks to the adjacent ground through the imperfect insulation, affecting the resulting induced voltages. This effect is expressed in terms of a coating shunt admittance Y_c, defined in S/m as:

$$Y_c = \frac{2\pi r_{ext}}{\rho_c \delta_c} + j\omega \frac{\varepsilon_0 \varepsilon_c 2\pi r_{ext}}{\delta_c}, \tag{6}$$

in which r_{ext} is the conductor external radius, in meters; ρ_c is the coating specific resistivity, in Ω.m; δ_c is the coating thickness, in meters; ε_0 is the vacuum electric permittivity, in F/m; and ε_c is the coating relative electric permittivity [1].

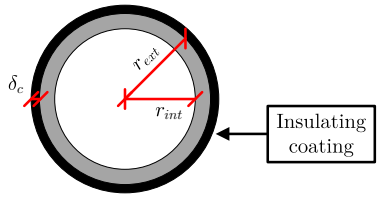

Fig. 3: Cross-section of a pipe with internal radius r_{int}, external radius r_{ext} and coating thickness δ_c.

D. Equivalent circuit EMTP/ATP model

The situation described in Fig. 1 and subsequent discussions corresponds to a perfect parallel approximation between conductors. However, more complex geometries, composed of combinations of obliquities, crossings and parallelisms, may occur in practical situations. Classically, such cases are constructed by subdividing the target installation into smaller segments that may be approximated by parallel sections, each one described by an equivalent length L_{eq} and distance D_{eq}, as Fig. 4 shows conceptually [1], [22].

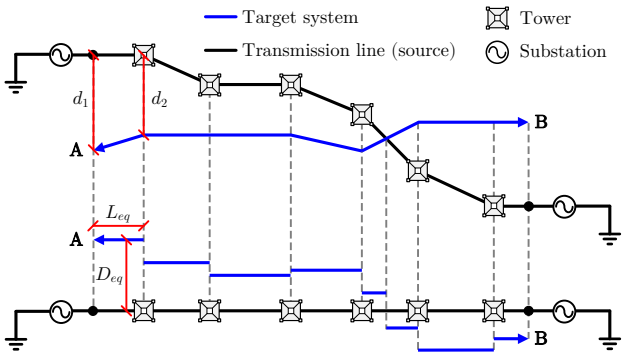

Fig. 4: Representation of a complex approximation in terms of equivalent parallel sections.

In this context, the subdivision scheme is a crucial factor that determines not only the accuracy of the induced voltage response, but the overall computational burden in the EMI simulation. The most comprehensible and well-documented subdivision procedure available in the literature, to the best of the authors' knowledge, is reported in [1]. Only a brief overview is given here, but its general idea consists of subdividing the target line sections into smaller portions,

according to the ratio between distances d_1 and d_2 shown in Fig. 4. There are two main points of concern with this approach: 1) even though it handles well situations with arbitrary target line paths, only the case of a perfectly straight transmission line route is considered in [1], whereas both the target and the transmission lines may follow jagged paths in practical situations; and 2) crossings or oblique approximations with sharp angles require a large number of subdivisions to be modeled accurately, which may render simulations using EMTP-type tools impractical.

To workaround these issues, a modified subdivision technique that accurately handles arbitrary line paths, which also produces a reduced number of segments, is proposed and tested in [22]. Fig. 5 describes one coupling region involving a transmission line and a target line, both of which may extend to the left and to the right outwards the coupling region and follow jagged pathways. Points T_1 and T_2 represent two adjacent towers, which define the straight line segment $\overline{T_1T_2}$ corresponding to one transmission line span with length L_1. Points P_1 and P_2 are the points contained in the target line with the minimum euclidean distances denoted by d_1 and d_2 to points T_1 and T_2, respectively. Points P_1 and P_2 define a curve segment $\overset{\frown}{P_1P_2}$ along the exposed line with length L_2, and also define a straight line segment $\overline{P_1P_2}$ that forms an angle θ with the transmission line span $\overline{T_1T_2}$. Then, the equivalent parallel exposure parameters are calculated using the well-known formulas discussed in [1], [24]:

$$D_{eq} = \sqrt{d_1 d_2}, \tag{7}$$

$$L_{eq} = \sqrt{L_1 L_2}\,|\cos\theta|\,, \tag{8}$$

with D_{eq}, L_{eq}, d_1, d_2, L_1, L_2 given in meters, and θ in degrees, according to the dimensions shown in Fig. 5.

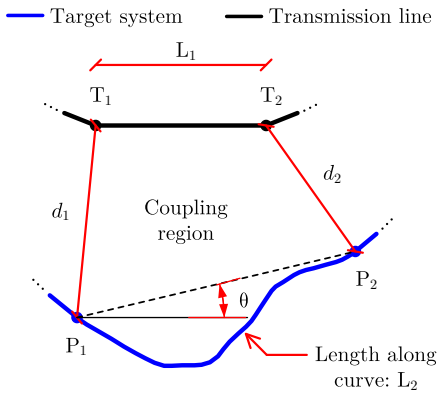

Fig. 5: Representation of a coupling region in the modified subdivision scheme.

Assuming the soil resistivity and the target conductor admittance to be constants along each coupling region, the circuit for one equivalent parallel section is built according to Fig. 6, which exemplifies the particular case (with no loss of generality) of a three-phase power line equipped with one shield wire, interfering with one target line, modeled using the ATPDraw interface. Two or even more shield wires may be modeled seamlessly, without changes to the resulting circuit representation, by attributing the different conductors to the same phase grounded at the extremities, and performing the bundle reduction operations reported in [25]. This process is handled automatically by ATP [15].

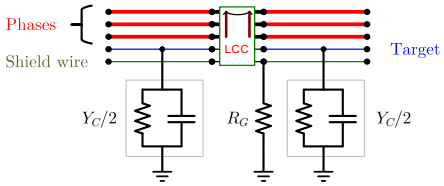

Fig. 6: ATPDraw representation of one section of a three-phase line with one shield wire and one interfered conductor.

The block labeled LCC represents the ATP routine Line/Cable Constants, which computes the corresponding conductor impedances from the system cross-section, material characteristics, soil resistivity and operating frequency, by using Carson equation (2). For the goals of this work, LCC objects are specified as nominal-π models, which agrees with the procedures established in the literature and implementations currently available in popular EMI simulation software [1], [26]. Components Y_c represent the pipeline coating and are calculated using (6). Ground resistances R_G at tower locations are determined from grounding electrode geometries and soil resistivities, by using appropriate numerical methods, or measured directly [27].

With the necessary parameters at hand, complex systems are built by successively concatenating the individual cells described above, process illustrated in Fig. 7 [22].

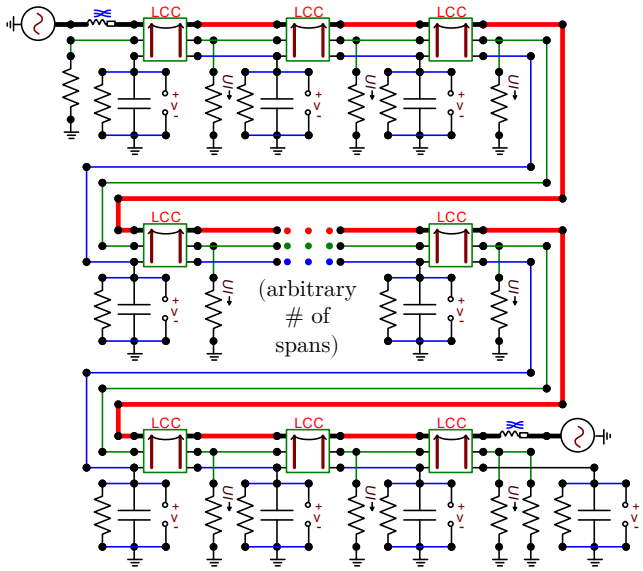

Fig. 7: ATPDraw representation of a complex approximation, in which each line span is modeled individually using LCC components.

III. Real case study

A. System description

The system object of study is a single-circuit, overhead, transposed 500 kV power line in Brazil, with an extension of approximately 300 km, interfering with a 28" underground gas pipeline, with a length of 448 km. The power line operates with a nominal load of 3800 A per phase.

At a given point, the two installations intersect each other, as shown in Fig. 8. Besides the crossing geometry, it can be observed that the pipeline follows a winding path, which is due to the terrain characteristics.

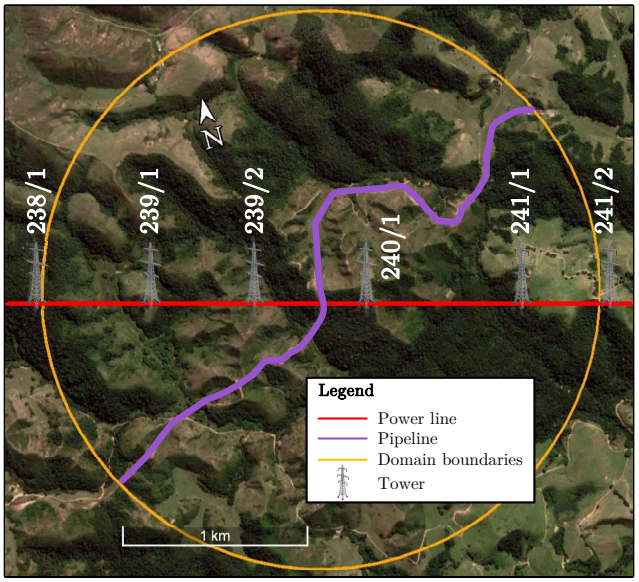

Fig. 8: Map of the approximation between a 500 kV transmission line and a 28" pipeline.

The domain of study is the orange circle with radius 1.5 km represented in Fig. 8. Outside the domain boundaries, the pipeline extends to far away from the power line, such that coupling effects become negligible and, in the equivalent circuit model, pipeline sections are replaced by their equivalent (characteristic) impedances, according to the directives given in [1]. Therefore, the region of interest is the pipeline section shown in purple, with an exposure length of 4.8 km.

The typical transmission line tower is the Guyed-type structure with the cross-section shown in Fig. 9. The average pipeline depth-of-cover is 1.5 m. Conductor specifications are given in Table I, in which R and X refer, respectively, to the AC resistance and reactance at 60 Hz, according to the catalogs from the manufacturers. Typical tower grounding resistance is 15 Ω.

TABLE I: Parameters of conductors.

Conductor	Outer radius [cm]	R [Ω/km]	X [Ω/km]
Phases	1.46177	0.068016	0.0199681
Shield wires	0.64008	0.486161	0.0186415
Pipeline	35.56	0.0496489	0.0495404

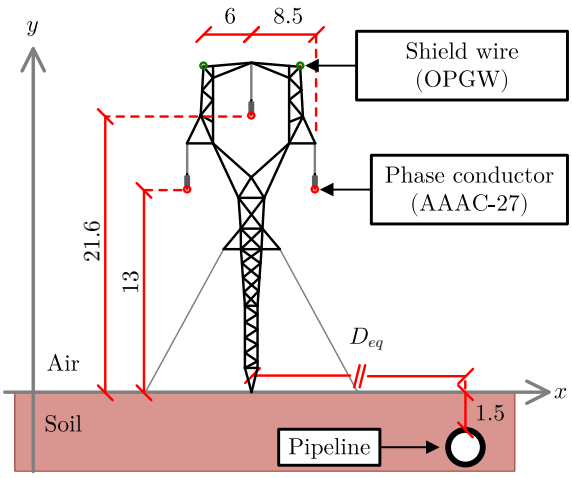

Fig. 9: Cross-section view of the system studied. All dimensions in meters.

Pipeline insulation material is three-layered polyethylene (3LPE), with thickness $\delta_c = 3$ mm, intrinsic resistivity $\rho_c = 10^{12}$ Ω.m and permittivity constant $\varepsilon_c = 2.25$, also according to design data.

B. Coupling regions and equivalent circuit model

In the complex approximation shown in Fig. 8, the transmission line in the vicinities of the winding pipeline path determines seven regions, identified by the numbers in Fig. 10. Regions one and seven (with the dotted lines), represent the pipeline and transmission line sections extending outwards the domain boundaries. Regions two to six model the sections effectively affected by EMI within the domain of study.

Then, referring to Fig. 11, the resulting circuit is comprised of seven cascaded LCC blocks representing the equivalent parallel approximations corresponding to each coupling region, according to the parameters shown in Table II. A relevant remark regarding the data contained in the table is that the equivalent exposure length L_{eq} does not necessarily express the actual physical dimensions along the power line (L_1) or along the pipeline (L_2). This is particularly evident at the crossing region, identified by number four, due to the almost orthogonal approximation between the installations involved, causing a substantial reduction in the mutual coupling effects, expressed numerically by L_{eq}.

When evaluating voltage profiles along the interfered installations, the use of L_{eq} as the spatial reference may lead to inaccuracies and distortions in the resulting curves. To address this issue, it is sufficient to observe, from Figs. 10 and 11, that each LCC node is uniquely mapped to one point along the transmission line and one point along the pipeline, and to adjust the distance axis accordingly.

C. Soil resistivity measurements

Soil resistivity data comes from actual field surveys performed at each tower location shown in Fig. 8, following the directives established in IEEE Std. 81 [28]. Apparent resistivity measurements were performed using the Wenner

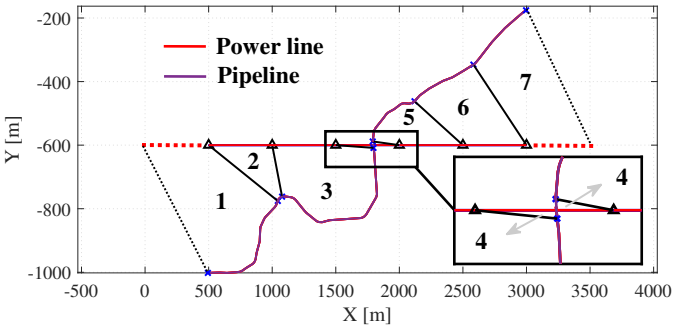

Fig. 10: Power line, pipeline and coupling regions.

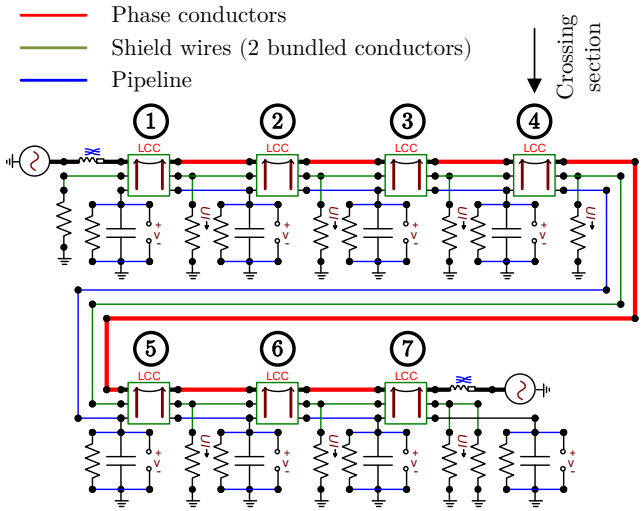

Fig. 11: Equivalent circuit of the system under investigation.

TABLE II: Parameters of the equivalent parallel sections.

Region	d_1 [m]	d_2 [m]	L_1 [m]	L_2 [m]	θ [°]	D_{eq} [m]	L_{eq} [m]
1	844.36	699.19	500	1420.86	22.12	768.35	780.82
2	699.19	412.53	500	47.78	45.28	537.06	108.76
3	412.53	297.25	500	1294.45	28.08	350.18	709.78
4	297.25	211.48	500	18.67	96.69	250.72	11.25
5	211.48	513.88	500	496.93	43.88	329.66	359.30
6	513.88	758.68	500	549.54	31.90	624.40	445.01
7	758.68	1067.38	500	922.01	30.50	899.89	585.00

four-pin method, at depths 1, 2, 4, 8, 16 and 32 m, along three different directions for each tower, making a total of 108 soil readings. The upper limit of 32 m was determined accordingly to field data, since it was found that performing additional readings, with larger electrode separations, did not produce significant changes in the resistivity of the deepest soil layers in the stratified results.

The soil model is constructed to represent the overall equivalent earth behavior within the domain of study. The procedure to account for the large dimensions involved consists of computing the 50% trimmed mean of apparent resistivity values for all tower locations shown in Fig. 8 at the corresponding depths, and then obtaining the layered soil parameters using the methods described in [29]. Apparent resistivity field data are summarized in Table III. The resulting soil model is composed of three layers, described by the parameters shown in Table IV and Fig. 12, with a fitting error of less than 3%. Clearly, the brown curve in Fig. 12 shows that the apparent resistivity values computed from the stratified soil parameters agree with the field measurements performed at each tower. Moreover, there is an excellent fit at the depth of 32 m (excluding the outlier from tower 239/2), indicating that the average behavior of the deepest soil layer is properly characterized, which is accurate enough for the purposes of this study [30].

TABLE III: Apparent resistivity summary at tower locations and trimmed mean values.

Depth [m]	238/1	239/1	239/2	240/1	241/1	241/2	Mean
	Apparent resistivity [Ω.m]						
1	544.48	490.23	466.79	396.47	604.75	567.94	517.36
2	743.96	632.75	598.24	526.65	778.48	778.48	688.36
4	1002.12	888.53	787.56	841.68	1081.30	1048.95	945.32
8	1177.50	1263.04	1016.47	1086.34	1410.68	1354.20	1220.27
16	1317.32	1186.59	1176.53	1084.31	1377.65	1327.36	1251.95
32	723.87	844.52	1045.59	731.19	764.09	797.00	784.20

TABLE IV: Parameters of the three-layered soil model

Layer	ρ [Ω.m]	h [m]	Reflection	Contrast
1	488.71	1.73	-1.00	0.00
2	2074.66	8.99	0.62	4.24
3	451.45	∞	-0.64	0.22

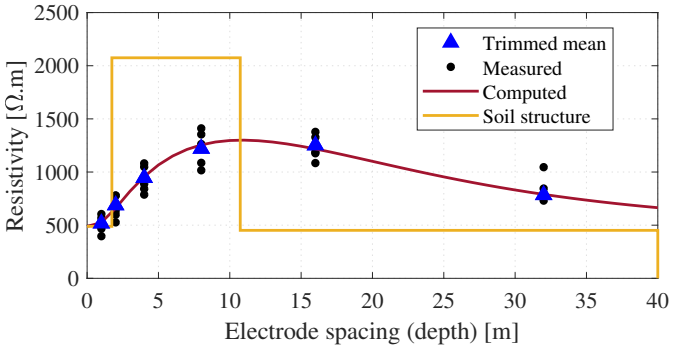

Fig. 12: Measured and computed soil resistivities.

Finally, Table V contains a comparison between three different uniform soil models: 1) the equivalent uniform model, determined using (3)-(5) and the data presented in Table IV; 2) the conventional uniform model, established under IEEE Std. 80 as the simple arithmetic mean of the apparent resistivity values [31]; and 3) the uniform model obtained using the RESAP module from software CDEGS, which is based on the curve-fitting technique reported in [32].

Examination of Tables IV and V shows that the equivalent uniform resistivity converges to the value of the deepest soil layer, with contrast ratios lower than 10, which are conditions for validity of the equivalent uniform approximation formula (3)-(5), as reported in [21]. Also, from Table V it is

TABLE V: Uniform resistivity values.

Model	Resistivity [Ω.m]
Equivalent uniform	456.14
Std. 80 uniform	1004.94
RESAP uniform	859.61

evident that the uniform parameters obtained using Std. 80 and RESAP approaches are of the order of 100% greater than the multilayered equivalent model, which is expected to drive the resulting voltages to increased values if these parameters are used in EMI calculations. This is further investigated in the following topic.

D. Simulation results

Assuming steady-state under nominal load conditions, simulations are executed to determine the voltages produced by the energized phase conductors on the pipeline due to inductive coupling, using the EMTP/ATP model and the equivalent soil approach described in the preceding sections.

For validation, results are compared with the professional software CDEGS, which effectively accounts for multilayered soils in calculations and is worldly-recognized as the industry-standard for EMI analysis [26].

Induced voltages as a function of the pipeline distance are shown in Fig. 13, as well as the results obtained using CDEGS software. The proposed approach agrees with the reference within a margin of less than 5 V at the worst profile point, with a RMS error of 8% between both responses and an excellent fit at the crossing location, where the pipeline induced voltage reaches its minimum value. On the other hand, the discrepancy more than doubles if the Std. 80 or RESAP uniform soil models are considered, with increased voltages and RMS errors of 22% and 19%, respectively, due to the higher resistivity values, showing how the soil model affects the outcome and may lead to conservative results and oversized designs.

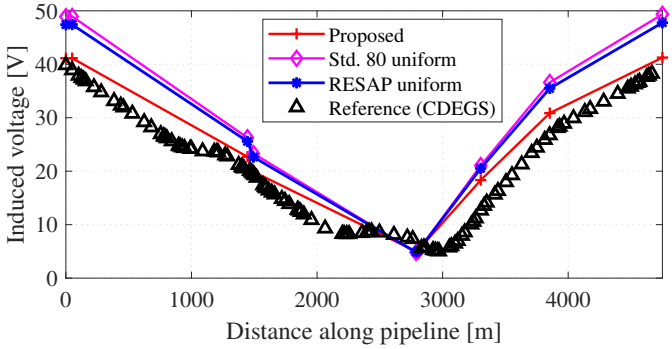

Fig. 13: Pipeline induced voltages under nominal load conditions.

Using the proposed approach, a maximum voltage of 41 V is found at the pipeline extremities, which far exceeds the safety limit of 15 V for pipelines, given under NACE standard SP0177-2007, and thus requires corrective measures [33]. One viable strategy to neutralize induced voltages is to ground the pipeline. In practice, this is accomplished by installing a buried bare copper conductor, known as mitigation wire, in parallel with the pipeline within the interference region. Then, the extremities of the pipeline are connected to the mitigation wire through solid-state decouplers, to prevent performance degradation of the cathodic protection systems usually employed to protect pipelines from corrosion. The effectiveness of this solution can be easily verified using the EMTP/ATP circuit model described in this work and shown in Fig. 11, by adding two low resistance values in parallel with the shunt impedances at the pipeline ends. Induced voltages are shown in Fig. 14, considering the pipeline to be grounded through resistances of 0.1 Ω. As in the original case, there is a good agreement between the resulting voltage profile and the reference curve. After the pipeline is grounded, the maximum induced voltage reaches only 10 V, which corresponds to a reduction of 75% in relation to the original case, thus complying with applicable safety standards.

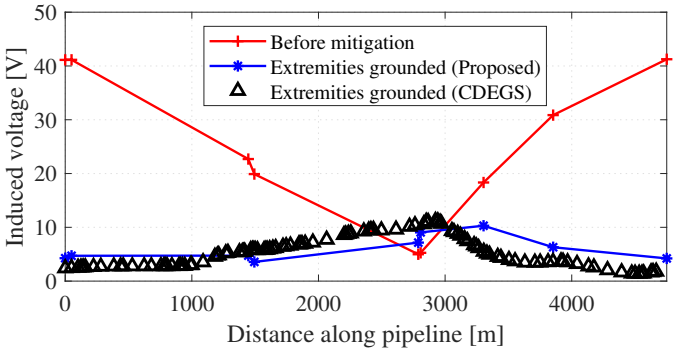

Fig. 14: Pipeline induced voltages before and after mitigation.

Some general remarks can be drawn from the analysis of induced voltages with respect to the soil resistivity. Voltages produced by inductive coupling mechanisms increase with the soil resistivity and depend fundamentally on the value of the deepest soil layer, as a closer inspection of (2) and (5) shows. Therefore, soil models that lead to higher resistivity parameters from the same set of field measurements tend to yield more conservative results, and the assumption of a uniform soil model based on apparent resistivities should be handled cautiously, as the response depends on the statistical behavior of the field measurements. For example, in the case of a soil structure composed of superficial layers with very low moisture content (dry sand) on top of large layers of hygroscopic material (humid clay), measurements performed at depths closer to the soil surface increase the arithmetic mean and, consequently, the uniform resistivity parameter and the resulting induced voltages. On the other hand, the actual voltage outcome determined using a true multilayered method, or the equivalent uniform formula described in this paper, will be more affected by the low resistivity due to water retention at the bottom layers, yielding significantly reduced voltage levels. In this extreme hypothetical scenario, a conservative approach may point to unrealistic violations of safety criteria, calling for unnecessary mitigation designs and elevated costs

with oversized grounding grids, decouplers etc.

IV. Conclusions

A case study of practical relevance to the industry was discussed in this paper, in which induced voltages on a 28" pipeline due to a neighboring 500 kV power line were computed using software EMTP/ATP and CDEGS.

Soil parameters are based on actual field data and resulted in a three-layered soil model. The horizontally stratified soil structure was accounted by means of a homogenization technique proposed and tested by the authors, which derives an equivalent uniform resistivity from N-layered soil parameters. An improved circuit model was used to represent the complex approximation between the power line and the pipeline, consisting of oblique exposures and one crossing point.

Induced voltages agreed with the reference steady-state values under a margin of less than 5 V, corresponding to a RMS error of 8%, and results emphasized the importance of properly accounting for the multilayered characteristic of natural soils in problems involving ground return impedances.

Moreover, resulting voltages exceeded the safety limits for pipelines and required corrective actions. Additional simulations were performed, with the pipeline grounded at the extremities, and showed a substantial reduction in the induced voltage values, thus ensuring compliance with applicable standards.

References

[1] CIGRÉ WG-36.02, "Technical Brochure n. 95 - Guide on the Influence of High Voltage AC Power Systems on Metallic Pipelines," Paris, pp. 1–135, 1995.

[2] J. I. R. I. Dabkowski and A. Taflove, "Mutual Design Considerations for Overhead AC Transmission Lines and Gas Transmission Pipelines Volume 1: Engineering Analysis," pp. 1–511, 1978.

[3] ——, "Mutual Design Considerations for Overhead AC Transmission Lines And Gas Transmission Pipelines Volume 2: Prediction and Mitigation Procedures," pp. 1–186, 1978.

[4] F. P. Dawalibi, R. D. Southey, Y. Malric, and W. Tavcar, "Power Line Fault Current Coupling to Nearby Natural Gas Pipelines: Volume 1, Analytic Methods and Graphical Techniques: Final report. EPRI-EL-5472-Vol.1. [Electromagnetic and Conductive Coupling Analysis of Powerlines and Pipelines (ECCAPP)]," United States, 1987.

[5] J. R. Carson, "Wave Propagation in Overhead Wires with Ground Return," *Bell Syst. Tech. J.*, vol. 5, pp. 539–554, 1926.

[6] F. Pollaczek, "On the Field Produced by an Infinitely Long Wire Carrying Alternating Current," *Electrische Nachrictentechnik*, vol. III, no. 9, pp. 339–359, 1926.

[7] E. D. Sunde, *Earth Conduction Effects in Transmission Systems*. New York, NY: Dover Publications, 1968.

[8] R. Heppe, "Computation of Potential at Surface Above an Energized Grid or Other Electrode, Allowing for Non-Uniform Current Distribution," *IEEE Transactions on Power Apparatus and Systems*, vol. PAS-98, no. 6, pp. 1978–1989, 1979.

[9] M. Nakagawa, A. Ametani, and K. Iwamoto, "Further Studies on Wave Propagation in Overhead Lines with Earth Return: Impedance of Stratified Earth," *Proceedings of the Institution of Electrical Engineers*, vol. 120, no. 12, p. 1521, 1973.

[10] G. Papagiannis, D. Tsiamitros, D. Labridis, and P. Dokopoulos, "A Systematic Approach to the Evaluation of the Influence of Multilayered Earth on Overhead Power Transmission Lines," *IEEE Transactions on Power Delivery*, vol. 20, no. 4, pp. 2594–2601, oct 2005.

[11] D. A. Tsiamitros, G. K. Papagiannis, P. S. Dokopoulos, and A. E. F. Equations, "Earth Return Impedances of Conductor Arrangements in Multilayer Soils - Part I: Theoretical Model," vol. 23, no. 4, pp. 2392–2400, 2008.

[12] A. Ametani, Y. Miyamoto, T. Asada, Y. Baba, N. Nagaoka, I. Lafaia, J. Mahseredjian, and K. Tanabe, "A Study on High-Frequency Wave Propagation along Overhead Conductors by Earth-Return Admittance / Impedance and Numerical Electromagnetic Analysis," in *Proc. IPST 2015*, Cavtat, Croatia, 2015.

[13] A. G. Martins-Britto, S. R. M. J. Rondineau, and F. V. Lopes, "Power Line Transient Interferences on a Nearby Pipeline Due to a Lightning Discharge," in *International Conference on Power Systems Transients (IPST 2019)*, Perpignan, France, 2019, p. 6.

[14] G. C. Christoforidis, D. P. Labridis, and P. S. Dokopoulos, "Inductive Interference Calculation on Imperfect Coated Pipelines Due to Nearby Faulted Parallel Transmission Lines," *Electric Power Systems Research*, vol. 66, pp. 139–148, 2003.

[15] H. W. Dommel, *EMTP Theory Book*. Microtran Power System Analysis Corporation, 1996.

[16] D. Caulker, H. Ahmad, and M. S. M. Ali, "Effect of Lightning Induced Voltages on Gas Pipelines using ATP-EMTP Program," in *2008 IEEE 2nd International Power and Energy Conference*. Johor Bahru, Malaysia: IEEE, 2008, pp. 393–398.

[17] B. Milesevic, B. Filipovic-Grcic, and T. Radosevic, "Analysis of Low Frequency Electromagnetic Fields and Calculation of Induced Voltages to an Underground Pipeline," in *Proceedings of the 2011 3rd International Youth Conference on Energetics (IYCE)*. Leiria, Portugal: IEEE, 2011, pp. 1–7.

[18] G. D. Peppas, M.-P. Papagiannis, S. Koulouridis, and E. C. Pyrgioti, "Induced Voltage on an Aboveground Natural Gas/Oil Pipeline Due to Lightning Strike on a Transmission Line," in *2014 International Conference on Lightning Protection (ICLP)*, no. 11. Shanghai, China: ICLP, 2014, pp. 461–467.

[19] S. Das, S. Santoso, A. Gaikwad, and M. Patel, "Impedance-based Fault Location in Transmission Networks: Theory and Application," *IEEE Access*, vol. 2, pp. 537–557, 2014.

[20] J. M. Whelan, B. Hanratty, and E. Morgan, "Earth Resistivity in Ireland," in *CDEGS Users' Group*. Montreal: Safe Engineering Services - SES, 2010, pp. 155–164.

[21] A. G. Martins-Britto, F. Lopes, and S. Rondineau, "Multi-layer Earth Structure Approximation by a Homogeneous Conductivity Soil for Ground Return Impedance Calculations," *IEEE Transactions on Power Delivery*, vol. 35, no. 2, pp. 881–891, 2020.

[22] A. G. Martins-Britto, "Realistic Modeling of Power Lines for Transient Electromagnetic Studies," Doctoral Thesis, University of Brasília, 2020. [Online]. Available: https://www.researchgate.net/publication/342916469_Realistic_Modeling_of_Power_Lines_for_Transient_Electromagnetic_Interference_Studies

[23] W. H. Dommel, "Digital Computer Solution of Electromagnetic Transients in Single- and Multiphase Networks," *IEEE Transactions on Power Apparatus and Systems*, no. 4, pp. 388–399, 1969.

[24] F. Dawalibi and R. Southey, "Analysis of Electrical Interference from Power Lines to Gas Pipelines. I. Computation Methods," *IEEE Transactions on Power Delivery*, vol. 4, no. 3, pp. 1840–1846, jul 1989.

[25] Y. Yang, J. Ma, and F. P. Dawalibi, "An Efficient Method for Computing the Magnetic Field Generated by Transmission Lines with Static Wires," in *Proceedings. International Conference on Power System Technology*, no. 2. Kunming, China: IEEE, 2002, pp. 871–875.

[26] F. P. Dawalibi and F. Donoso, "Integrated Analysis Software for Grounding, EMF, and EMI," *IEEE Computer Applications in Power*, vol. 6, no. 2, pp. 19–24, 1993.

[27] F. Dawalibi and N. Barbeito, "Measurements and Computations of the Performance of Grounding Systems Buried in Multilayer Soils," *IEEE Transactions on Power Delivery*, vol. 6, no. 4, pp. 1483–1490, 1991.

[28] IEEE, "Guide for Measuring Earth Resistivity, Ground Impedance, and Earth Surface Potentials of a Ground System," New York, NY, p. 86, 2012.

[29] T. Takahashi and T. Kawase, "Analysis of Apparent Resistivity in a Multi-Layer Earth Structure," *IEEE Transactions on Power Delivery*, vol. 5, no. 2, pp. 604–612, 1990.

[30] R. Southey and F. Dawalibi, "Improving the Reliability of Power Systems with More Accurate Grounding System Resistance Estimates," *Proceedings. International Conference on Power System Technology*, vol. 4, pp. 98–105, 2005.

[31] IEEE, "Guide for Safety In AC Substation Grounding," p. 226, 2013.

[32] F. Dawalibi and C. Blattner, "Earth Resistivity Measurement Interpretation Techniques," *IEEE Transactions on Power Apparatus and Systems*, vol. PAS-103, no. 2, pp. 374–382, 1984.

[33] NACE, "SP0177-2007 - Mitigation of Alternating Current and Lightning Effects on Metallic Structures and Corrosion Control Systems," pp. 1–25, 2007.